Full paper

Smart liquid-piston based triboelectric nanogenerator sensor for real-time monitoring of fluid status☆

Taotao Zhan [a,1], Haiyang Zou [b,c,1], Hengfei Zhang [a], Peng He [a], Zhanlei Liu [d], Junshuai Chen [a], Maogang He [a], Ying Zhang [a,*], Zhong Lin Wang [c,e,**]

[a] Key Laboratory of Thermo–Fluid Science and Engineering, Ministry of Education, Xi'an Jiaotong University, Xi'an 710049, China
[b] College of Materials Science and Engineering, Sichuan University, Chengdu 610065, China
[c] School of Materials Science and Engineering, Georgia Institute of Technology, Atlanta 30332, USA
[d] School of Electrical Engineering, Xi'an Jiaotong University, Xi'an 710049, China
[e] Beijing Institute of Nanoenergy and Nanosystems, Chinese Academy of Sciences, Beijing 101400, China

ARTICLE INFO

ABSTRACT

It is highly desirable to measure fluid pressure and its pulsations through portable, handheld instruments and test kits, which allow a rapid, low-cost, and reliable quantification about liquid status, especially for cheaper, faster, and smarter point-of-care testing (POCT). Here, we proposed a portable self-powered smart fluid pressure sensor based on a liquid piston triboelectric nanogenerator (LP-TENG). By analyzing the characteristic signals due to the triboelectrification effect, electrostatic induction, and theory of the ideal gas equation, the developed sensor is able to determine the fluid's pressure and flowing status quantitatively (e.g., moving direction, flow rate, blockages, pipe bursts, leakage, etc.). Here, a simply fabricated device has the highest accuracy of 0.4 kPa with a pressure range from 0 kPa to 30 kPa, which is superior to most commercial sensors. Furthermore, the electric performance can reach a resolution ratio of 10 mmHg, which is adequate to accurately identify the blood pressure (BP) level. Consequently, the self-powered LP-TENG is capable of real-time monitoring the fluid status, which can fit the need for diagnosing and detecting the BP level as a reliable POCT device in healthcare products, as well as other broad potential applications in manufacturing, transportation, and civil service.

1. Introduction

With increasing urbanization, sensors, as vital components for monitoring and control of the environment and individual states, have been used in the architectures of industrial automation, intelligent manufacturing, Internet of Things (IoT), and health devices [1–4]. Fluid pressure sensors are essential to track the working, operating, or health conditions for real-time monitoring in fluid lines. Especially for the biosensors in smart analytical diagnostic tools, they have been widely investigated with the potential of point of care testing (POCT) needed for personalized health care/management. Compared to a competent system of laboratory diagnostics, affordable portable self-powered pressure sensors with low-cost and multi-functions are always required in terms of progression and monitoring evaluation that produces rapid and reliable results. The existing flow sensors include two groups of contact and non-contact sensors. The liquid directly contacts the sensor's moving part (i.e., a small latch in vortex flow sensors, and propellers in mechanical flow sensors). The most popular non-contact fluid sensor is the ultrasonic flow sensor, which sends pulses of high-frequency sound across the flowing liquid medium, and measures the time difference between the emission and receiver to determine the flow rate. These costly instruments are complex and difficult to handle due to their size or weight. Most of the existing pressure sensors like the electronic or mercury sphygmomanometers are difficult to recycle. The integrated

circuit of sensors for monitoring multi-parameters of fluid status requires complex systems to power, send and receive signals, and analyze data.

Under these circumstances, the triboelectric nanogenerator (TENG) with the advantages of self-powered capacity, lightweight, online detection, and extremely high sensitivity, is becoming an attractive alternative for sensor manufacturing [5–9]. Moreover, regarding the connection between human beings and the environment, several self-powered sensors based on liquid-solid TENG have been proposed [10–14], to determine the physicochemical properties of the fluid medium such as pressure [15,16], temperature [17], humidity [18], and chemical composition [19,20]. Among liquid-solid TENGs, tube-based TENG (TB-TENG) has attracted great interest from researchers [15, 21–25]. According to the type of liquid volume, there are tube-based TENGs with the liquid of infinite volume (IV-TB-TENG) and that with the liquid of finite volume (FV-TB-TENG) to meet various application requirements. For the IV-TB-TENG, typically, a ring-type or an intertwined electrode arranged outside the tube and a grounded reference electrode are normally adopted [15,22]. Besides, a remote electrode or an adjacent electrode is regarded as a reference electrode, and several electrodes are used to detect the volume of the internal liquid [21,25, 26]. As for the FV-TB-TENG, the electrode doublet is normally used to determine the liquid movement in U-tube TENG with the charge transfer between the reference electrode and the sensing electrode [23,24,27, 28]. As a concluding point, compared with FV-TB-TENG, the IV-TB-TENG using the liquid with infinite volume is normally larger, of which the portability is less competitive. Besides, for the IV-TB-TENG, because of the residual liquid on the inside tube wall after the liquid
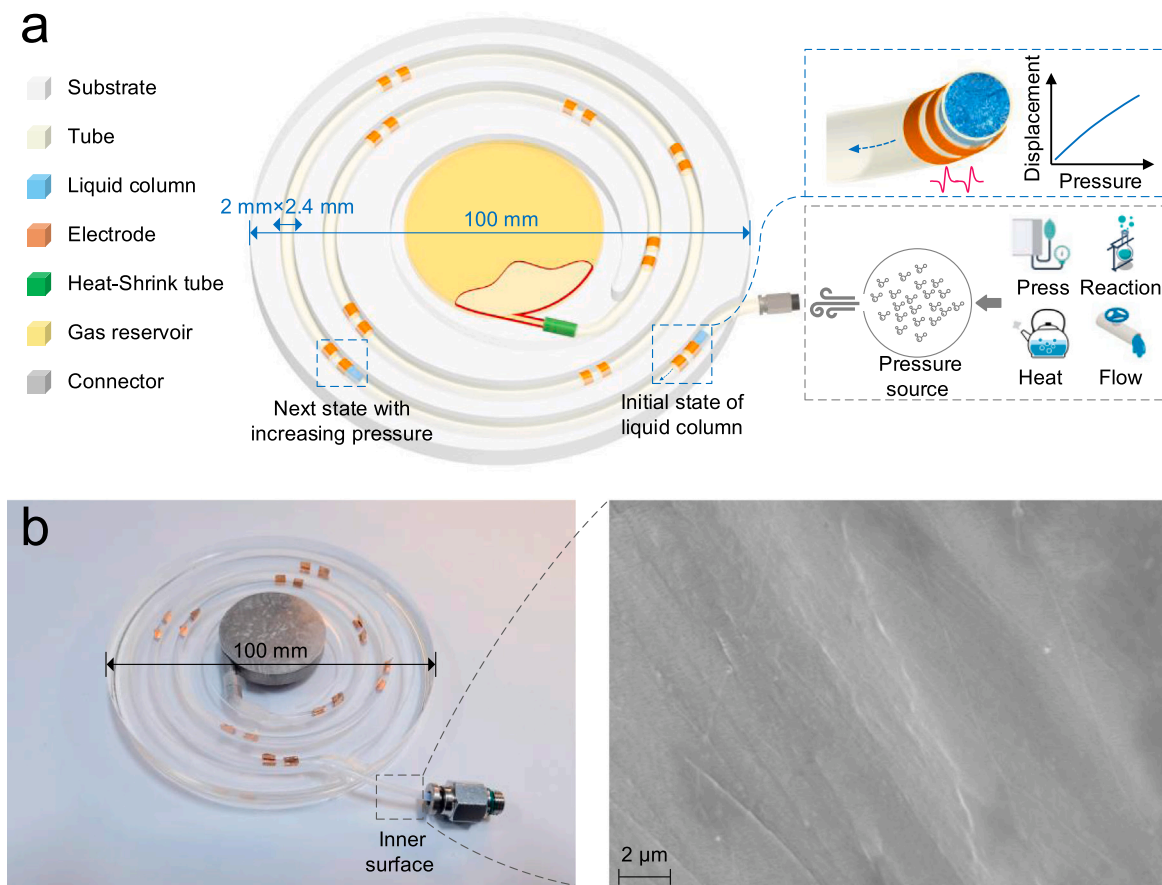
column crosses the electrodes, the electrical signal would be not easy to repeat. Although diverse structures and designs are proposed for sensing, it is still challenging to determine the fluid flow status (flow rate, direction, pressure, etc.) by a single simple device.

In this work, a liquid-piston based triboelectric nanogenerator (LP-TENG) using the FV-TB-TENG design for fluid flow monitoring is proposed. The LP-TENG is simply composed of a tube, a liquid column, electrodes, and an air reservoir. The liquid column is considered to be a piston in the tube attached to the air reservoir, and movement-related electrical signals due to the triboelectric effect can be obtained from electrode arrays with a single channel detector based on the triboelectric effect, the electrostatic induction effect, and the theory of the ideal gas equation. The fabricated LP-TENG has been demonstrated to measure human blood pressure, which has superior performance than other commercial products. Furthermore, by designing various electrode arrays and a developed computer program, the smart sensor is able to identify the flowing rate, direction, and pressure change as demonstrated. Consequently, the LP-TENG has the potential to act as a stable and reliable pressure sensor for other applications, such as health monitoring and diagnosis, manufacturing, and transportation.

2. Results and discussion

2.1. Concept design and working principle of LP-TENG

The real-time monitoring of fluid flow status is essential for daily life and industry. Flow sensors are commonly used in heating, ventilation and air conditioning (HVAC) systems, medical devices, chemical

Fig. 1. Structural design of the proposed LP-TENG. (a) Schematic drawing of the LP-TENG with four pressure sources of press, reaction, heat, and flow. The liquid column is crossing electrodes under the elevated pressure, and it is generating electrical output. (b) Tilted view photograph of LP-TENG with the image of the scanning electron microscope (SEM) of the inner surface of a PTFE tube, after ultrasonically cleaned in ethanol for 8 mins, and then left in the drying oven at 40 ℃ for 30 mins.

factories, and septic systems for detecting leaks, blockages, pipe bursts, and changes in liquid concentration due to damage, contamination, or pollution. Fig. S1 depicts four application scenarios including hospital, factory, vehicle, and pipeline. The schematic drawing of the LP-TENG with four pressure sources of press, reaction, heat, and flow is illustrated in Fig. 1. As has been shown, the LP-TENG is mainly composed of the air reservoir and the FV-TB-TENG which consists of a polytetrafluoroethylene (PTFE) tube, the liquid column, and multiple Cu electrodes. Here, a commercial PTFE tube and the deionized water liquid column serve as a friction pair of TENG. The polydimethylsiloxane

(PDMS) structure layer is used to be a structural foundation. It should be noted that the metal chamber, considered a gas reservoir, is made of titanium alloy manufactured by a 3D printer. In addition, the heat-shrink fluorinated ethylene propylene (FEP) tube connector is used to connect the metal chamber to the PTFE tube. The silicone or steel tube connector is connected to the PTFE tube with the pressure source, and the inner area of the PTFE tube between the liquid column and the metal chamber is filled with air. Before starting the measurement, the PTFE tube is disconnected to the gas reservoir, and then the liquid column is injected into the PTFE tube. After that, the PTFE tube can be connected
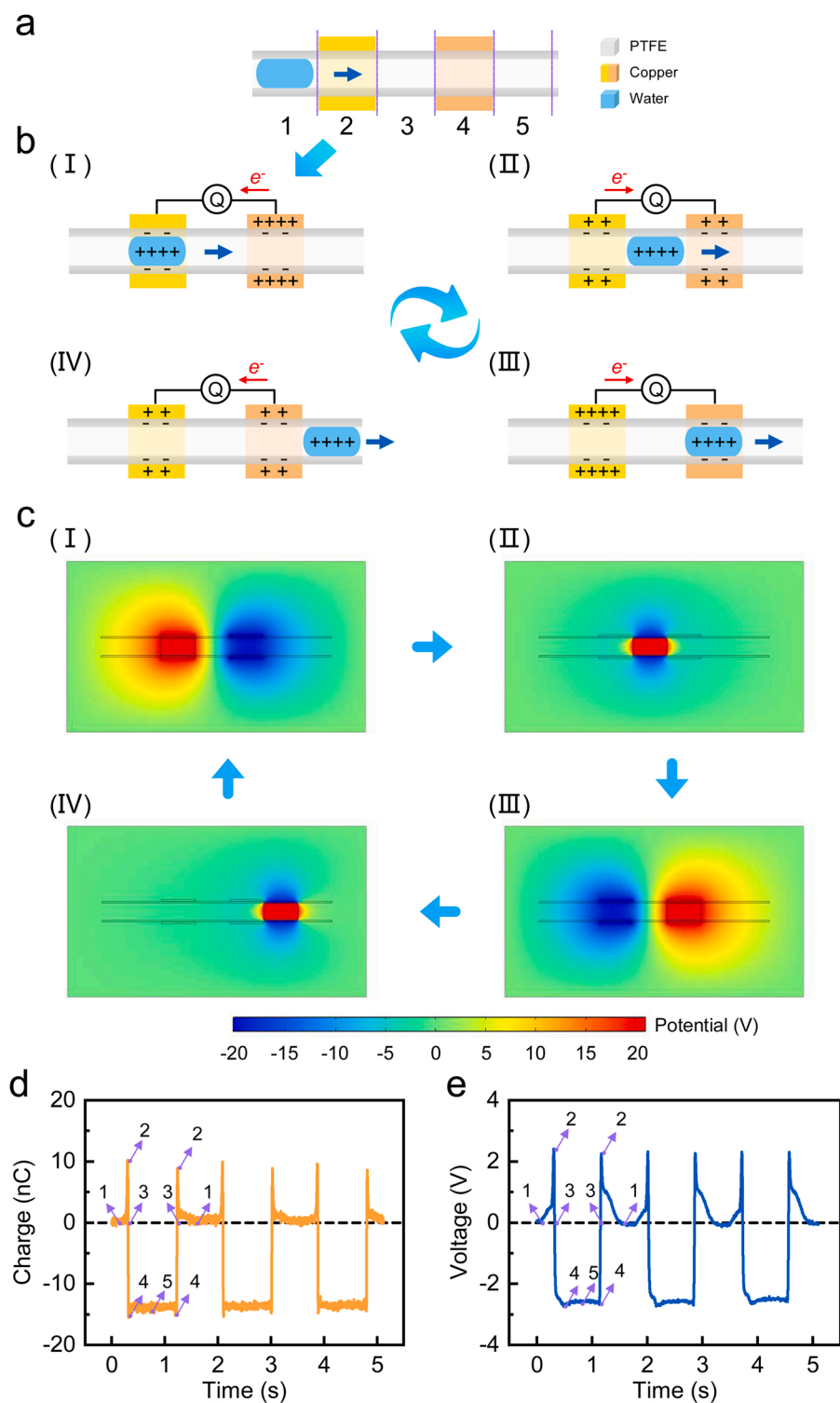
Fig. 2. Charge transfer mechanism and the working principle of the tube-based TENG of LP-TENG with the liquid column crossing the electrode doublet. (a) Definition of the tube-based TENG with five divided areas. (b) Transferred charge. (c) Potential field. (d-e) Typical experimental transferred charges and open-circuit voltages (V_{OC}) with the liquid column moving forward and backward by three times. The number represents the liquid column fully enters the corresponding area from left to right and then from right to left.

to the gas reservoir by using the FEP tube connector. In Fig. 1a, when the LP-TENG is connected to a pressure source, the liquid column, as a liquid piston, would move forward or backward into the metal chamber until there is no pressure differential between the pressure of the pressure source and that of air inside the air reservoir and the PTFE tube. Hence, the pressure of a pressure source can be determined according to the triboelectrification between the liquid column and the inner wall of a PTFE tube and the electrostatic induction between the PTFE tube and Cu electrodes. The tilted view photograph of the LP-TENG with the image of the scanning electron microscope (SEM) of the inner surface of a PTFE tube is shown in Fig. 1b.

The charge transfer mechanism and the working principle of the FV-TB-TENG of LP-TENG are illustrated in Fig. 2. The definition of the FV-TB-TENG components is shown in Fig. 2a. Under a certain pressure difference, the liquid column would have a specific displacement in the PTFE tube to enter or leave the electrode-covered region. Fig. 2b shows the transferred charges of the FV-TB-TENG with the liquid column at different positions. The whole system is equivalent to a series of two capacitors. One is from the contribution of an outer electrode, the air, and water, and the other is attributed to the PTFE dielectric. When the liquid column is not in the area of Cu electrodes, there is no potential difference between the two electrodes as no electrostatic induction happens in the electrode areas, and it has no voltage output. When the liquid column moves forward to position I, the internal wall of the PTFE tube is triboelectrically negatively charged due to the relative motion.

To maintain static electricity conservation, the positive charges in the first electrode would move to the second electrode and generates the current. When the liquid column continues to move forward to position II, the charge in the electrodes will be redistributed, and a current opposite will be generated at this time. If the liquid column continues to flow forward to position III, the positive charges in the second electrode will move to the first electrode. Furthermore, when the droplet moves forward to position IV, the charges in the electrodes will be reset, and the current that is opposite to that of state III will be generated at this time. To qualitatively verify the above inference, the potential field of the FV-TB-TENG was simulated by COMSOL. Fig. 2c illustrates the potential field of the FV-TB-TENG when the liquid column is at a different position. The variation of the potential field with different liquid column movements is analogical to that of the transferred charge. Here, under open-circuit conditions, the positive charges induced by water will not move to the other electrode, and the potential of the electrode covering the liquid column will be significantly higher than that of the other electrode. Finally, the liquid column displacement sensing can be realized by arranging electrodes on the outer wall of a PTFE tube. Fig. 2d and e depict typical experimental transferred charges and open-circuit voltages (V_{OC}) when the liquid column is moving forward and backward by three times. The number represents the liquid column fully entering the corresponding area from left to right and then from right to left shown in Fig. 2a.

2.2. Theoretical modeling of LP-TENG

A theoretical model of thermodynamics is constructed to further explain the mechanism of pressure sensing by LP-TENG. The relationship between the displacement of the liquid column and the pressure of air is governed by the equation of state for air. Here, the ideal gas equation of state is employed in the modeling process. According to the law of conservation of mass, the pressure of the inside air in a gas reservoir can be represented by, $p = p_0 V_0 / (V_0 + xS)$, where p indicates the pressure of air when the liquid piston is moving, p_0 is the pressure of inside air when the liquid piston is under the initial situation, V_0 is the volume of inside air when the liquid piston is under the initial situation, x is the displacement of the inside air, and S is the area of the inside area of the PTFE tube. If p is higher than p_0, the liquid piston will move forward to the gas reservoir, and the positive charges from the first electrode will move to the second electrode. Besides, if p is lower than p_0,

the liquid piston will move backward to the metal chamber, and the positive charges from the second electrode would move to the first electrode. Finally, the pressure of a pressure source and that of air inside the air reservoir and the PTFE tube would reach equilibrium.

2.3. Electrical characterization of LP-TENG

The influences of the inner diameter of the tube, D, the electrode length, W, the distance between electrodes, H, the length of the liquid column, L_{liq}, and the velocity of the liquid column, u, on the electrical output of the FV-TB-TENG of LP-TENG have been systematically investigated, as illustrated in Fig. 3. Fig. 3a depicts a stepping motor-driven experimental system with a PTFE tube connecting to the environment for characterizing the output of the FV-TB-TENG. The motor drives the plunger rod of the syringe to simulate the pressure difference, and then to drive the movement of the liquid column, and its outputs under various conditions can be determined. Fig. 3b and Supplementary Video S1 show the V_{OC} over the time when the liquid column is crossing the positive electrode and the negative electrode. When the liquid column is crossing the electrode doublet, the V_{OC} first increases up to 1.4 V, and then decreases sharply to -1.7 V when it goes to the negative electrode. The open-circuit voltage and the transferred charge with different velocities of the liquid column are offered in Fig. 3c. With the u grows from 4.8 mm·s^{-1} to 240 mm·s^{-1}, the open-circuit voltage difference between the maximum voltage and the minimum voltage, $V_{OC, D}$, increases from around 0.4–2.9 V with a high signal-to-noise ratio. The $V_{OC, D}$ increases slowly with increasing velocity when the u is larger than 40 mm·s^{-1}, which means the surface charges due to the triboelectric effect between the liquid column and the PTFE tube reaches a saturation point. Fig. S2 shows the open-circuit voltage differences with different liquid columns' velocities. Fig. 3d depicts the variations in the $V_{OC, D}$ and the transferred charge Q_D with different inner diameters of the PTFE tube. As can be seen, both the $V_{OC, D}$ and Q_D increase significantly as the inner diameter of tube D varies from 1.5 mm to 3.0 mm. The impact of D on the output becomes less important when it goes above 3 mm. Fig. 3e shows the variations in the $V_{OC, D}$ when the electrode length, W, and the length of the liquid column, L_{liq}, both change from 1 mm to 7 mm at the distance between electrodes, H, of 4 mm. With increasing L_{liq}, the $V_{OC, D}$ would first increase and then decrease, which means the FV-TB-TENG would reach maximum electrical output when the length of the liquid column equals that of the electrode. Fig. 3f shows the variations in the $V_{OC, D}$ when the distance between electrodes, H, and the length of the liquid column, L_{liq}, both change from 1 mm to 7 mm at the electrode length, W, of 4 mm. With increasing L_{liq} and decreasing H, the $V_{OC, D}$ would increase. To sum up, it is readily apparent that with the smaller electrode spacing, the longer electrode length, and the longer liquid column length, the V_{OC} of the FV-TB-TENG would be larger. As can be seen, when the L_{liq} increase from 2 mm to 3 mm, the $V_{OC, D}$ will increase from around 1–2 V with a huge variation, and the D only has a little influence on the $V_{OC, D}$. With the comprehensive consideration of the electrical performances, the resolution of LP-TENG, and the size of the fabricated devices, the PTFE tube with the inner diameter of 2 mm was adopted, and the electrode length, W, and the length of the liquid column, L_{liq}, and the distance between electrodes, H, were all taken as 3 mm.

Supplementary material related to this article can be found online at doi:10.1016/j.nanoen.2023.108419.

### 2.4. Characteristic signals of FV-TB-TENG based on electrode array structures

The output performance of FV-TB-TENG with different electrode array structures is investigated to explore the multi-functions of FV-TB-TENG. Here we mark the electrodes connected to the positive side of the electrical meter as "positive", and the negative side as "negative". Fig. 4 shows the open-circuit voltages of the FV-TB-TENG with positive-
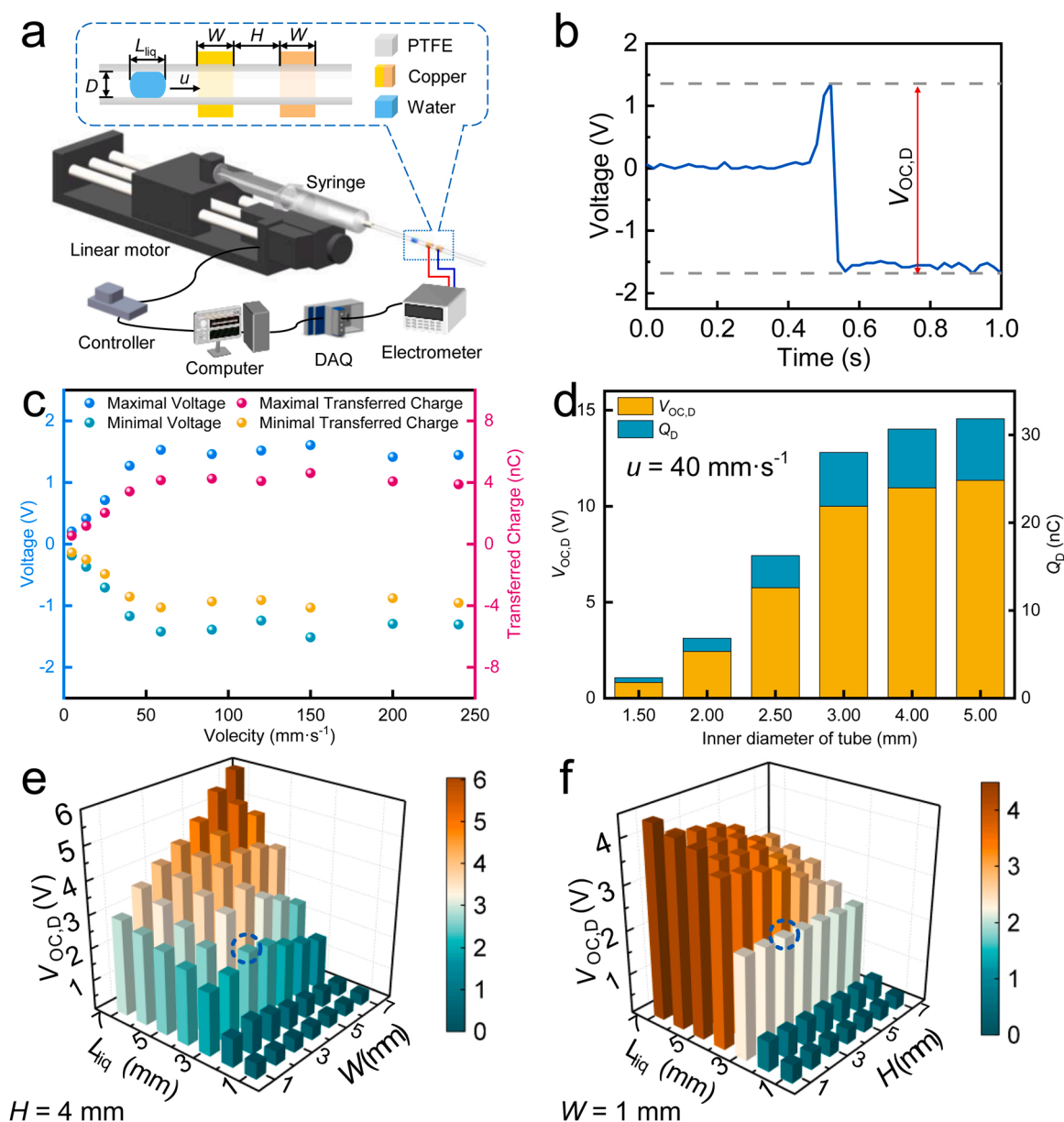
Fig. 3. Parameter optimization and electrical performances for the tube-based TENG of LP-TENG with the liquid volume crossing the electrode doublet. (a) A stepping motor-driven experimental system for determining the output performance of the tube-based TENG. (b) Variations in the V_{OC} with the liquid column crossing the electrode doublet. (c) The open-circuit voltages and the transferred charges with different velocities of the liquid column. (d) Variations in the open-circuit voltage difference between the maximum voltage and the minimum voltage ($V_{OC,\ D}$) and the transferred charge with different inner diameters of PTFE tube, D. (e) Variations in the $V_{OC,\ D}$ when the electrode length, W, and the length of the liquid column, L_{liq}, change from 1 mm to 7 mm with the distance between electrodes, H, of 4 mm. (f) Variations in the $V_{OC,\ D}$ when the distance between electrodes, H, and the length of the liquid column, L_{liq}, change from 1 mm to 7 mm with the electrode length, W, of 4 mm. With the comprehensive consideration of the electrical performances and the resolution of LP-TENG, the PTFE tube with the inner diameter of 2 mm was adopted, and the electrode length, W, and the length of the liquid column, L_{liq}, and the distance between electrodes, H, were taken as 3 mm.

negative + negative-positive (PN+NP), negative-positive + positive-negative (NP+PN), positive-negative-positive + negative-positive-negative (PNP+NPN) electrode arrays by a forward movement (FM) or a backward movement (BM). For these electrode arrays, if the liquid column goes back to its original position by BM, a similar signal series would be obtained compared with that of FM. For the PN+NP electrode array, as shown in Fig. 4a, the maximum V_{oc} are 1.65 V and 2.20 V, and the minimum V_{oc} are − 2.07 V and −2.26 V for FM and BM, respectively. The absolute value of maximum V_{oc} and that of minimum V_{oc} are close. However, for the NP+PN electrode array, as shown in Fig. 4b, the maximum V_{oc} are 2.68 V and 3.43 V, and the minimum V_{oc} are − 0.84 V and − 0.81 V for FM and BM, respectively. The absolute value of

maximum V_{oc} is much higher than that of minimum V_{oc}. As a combination of PN+NP and NP+PN, the PNP+NPN electrode array, as shown in Fig. 4c, the maximum V_{oc} of P3 (1.75 V or 1.58 V) is much higher than that of P1 or P2 (0.78 V or 0.97 V), and the minimum V_{oc} of N1 (−1.07 V or −0.78 V) is much smaller than that of N2 or N3 (−0.29 V or −0.19 V). As can be seen in Fig. 4, if only multiple PN+NP or NP+PN electrode arrays were used, it is difficult to determine the direction the liquid column movement. However, with multiple PNP+NPN electrode arrays, if the liquid column moves by a FM, the minimum V_{oc} comes first and then the maximum V_{oc} comes. If the liquid column moves by a BM, the maximum V_{oc} comes first and then the minimum V_{oc} comes. As can be seen, the V_{oc} signal of the FV-TB-TENG
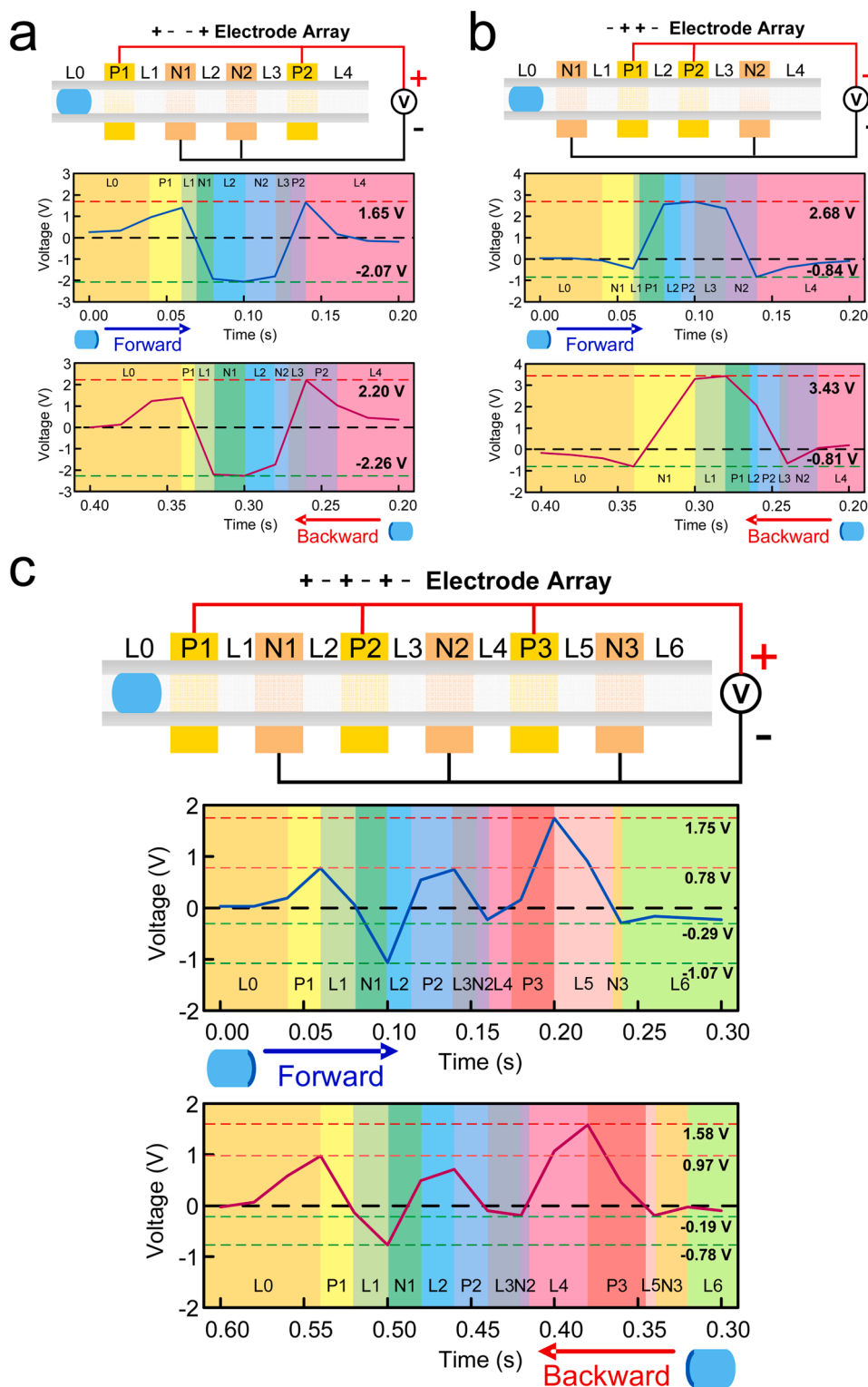
Fig. 4. Triboelectric performance of the tube-based TENG of LP-TENG with different electrode arrays when the liquid column is in a forward movement (FM) or a backward movement (BM). (a) The positive-negative + negative-positive (PN+NP) electrode array. (b) negative-positive + positive-negative (NP+PN) electrode array. (c) The positive-negative-positive + negative-positive-negative (PNP+NPN) electrode array.

using the PNP+NPN electrode array is very stable and there is no zero-point shift, which means the PNP+NPN electrode array can be used to determine the direction and the displacement of the liquid column movement simultaneously. Fig. S3 depicts the open-circuit voltages of FV-TB-TENG when the liquid column crosses the PTFE tube with the positive-negative + positive-negative (PN+PN) electrode array. The

experiments with the PN+PN, PN+NP, NP+PN, and PNP+NPN electrode arrays are demonstrated in Supplementary Video S2. Therefore, we could design various electrode array structures for detecting multi-parameters of the fluid status, e.g., flowing direction, pressure, flow-ing rate, etc. Fig. S4 depicts the typical and ideal voltages of the LP-TENG with the positive-negative (PN), the negative-positive (NP), the

positive-negative-positive (PNP), and the negative-positive-negative (NPN) electrode array.

Supplementary material related to this article can be found online at doi:10.1016/j.nanoen.2023.108419.

3. Applications

Some further demonstrations of its practical applications are illustrated in Fig. 5. The pressure sensing characteristics of LP-TENG employing a PNP+NPN electrode array are presented and analyzed in Fig. 5a-e. Fig. 5a provides a schematic representation of the testing setup for the LP-TENG pressure sensing. The center position of the middle electrode of electrode arrays is determined based on the corresponding pressure. A stepping motor is adopted to provide the pressure source by directing the movement of the syringe plunger, and a commercial manometer is used as a reference detector for comparison. The relationship between the displacement of the liquid column and the determined pressure of LP-TENG is shown in Fig. 5b. As a result, the displacement of the liquid column will rise from 0 mm to 454 mm with a pressure range from 0 kPa to 30 kPa. Hence, the relationship between the displacement of the liquid column and measured pressure is compatible with the ideal gas state equation with a deviation of ± 0.26 kPa. Software for obtaining and analyzing the characteristic signals is developed. Fig. 5c illustrates the V_{OC}, square-modulated (SM) voltage, peak-modulated (PM) voltage, latest peak-modulated (LPM) voltage, movement direction (MD), and the determined pressure of LP-TENG when the liquid column is crossing the PNP+NPN electrode array with the forward and then backward movement. The algorithm of LP-TENG for determining the moving direction and the moving displacement of the water column as a pressure sensor is shown in Fig. S5.

The voltage signal is transferred to the square-modulated voltage using a high threshold voltage of 3.0 V and a low threshold voltage of -1.0 V. If the V_{oc} is lower than -1.0 V, the square-modulated voltage equals -1 V. If the V_{oc} is higher than 3.0 V, the square-modulated voltage equals 1 V. If the voltage is between -1.0 V and 3.0 V, the square-modulated voltage equals 0 V. As a result, the sign of entering the negative electrode of the PNP electrode array and that of entering the positive electrode of the NPN electrode array can be obtained. Moreover, to obtain the position of the liquid column more precisely, the square-modulated voltage is transferred to the peak-modulated voltage. If the square-modulated voltage is changed from 0 V to -1 V, the peak-modulated voltage equals -1 V. If the square-modulated voltage is changed from 0 V to 1 V, the peak-modulated voltage equals 1 V. Otherwise, the peak-modulated voltage equals 0 V. Hence, the exact time of the liquid column crossing the positive electrode of the NPN electrode array and that of the liquid column crossing the negative electrode of the PNP electrode array can be obtained. Furthermore, in order to determine the movement direction of the liquid column, the peak-modulated voltage is transferred to the latest peak-modulated voltage. If the peak-modulated voltage changes from 0 V to 1 V or from 0 V to -1 V, the latest peak-modulated voltage equals the newest peak-modulated voltage. Otherwise, the latest peak-modulated voltage with an initial value of 0 V equals its previous value. First, the latest peak-modulated voltage changes from 0 V to -1 V when the liquid column crosses the negative electrode of the NPN electrode array by FM. Then, the latest peak-modulated voltage changes from -1 V to 1 V when the liquid column crosses the positive electrode of the PNP electrode array by FM. Afterward, the latest peak-modulated voltage remains at 1 V when the liquid column crosses the positive electrode of the PNP electrode array for the second time by BM. Finally, the latest peak-modulated voltage changes from 1 V to -1 V when the liquid column crosses the negative electrode of the NPN electrodes for the second time by BM. Moreover, the movement direction for the liquid column can be determined from the latest peak-modulated voltages. If the peak-modulated voltage changes from 0 V to 1 V or from 0 V to -1 V, and the peak-modulated voltage equals the latest peak-modulated voltage,

the movement direction of the liquid column changes. Otherwise, the movement direction of the liquid column does not change.

Fig. 5d depicts the comparison of the accuracy and the maximum pressure between LP-TENG with the PN+PN electrode array and several commercial products and literature results. By using the PN+PN electrode array with all the electrode length, the length of the liquid column, and the distance between electrodes taken as 3 mm, the length of electrode combined with the space between two electrodes is 6 mm. Because every positive and negative electrode can provide pressure signal, the accuracy of LP-TENG can be estimated as $6/454 \times 30$ kPa = 0.4 kPa. Hence, the LP-TENG is confirmed to be commercially competitive with a maximum pressure of 30 kPa. In the previous work from Sang et al. [15], the detected minimum pressure difference of a tube-based triboelectric nanogenerator was 0.49 kPa. Fig. S6 depicts physical images of the testing setup for the LP-TENG pressure sensing. The initial value is 0 kPa, and the pressure difference between the middle electrode of the PNP electrodes and that of the NPN electrodes is 5 kPa. If the peak-modulated voltage changes from 0 to 1 V or -1 V, the pressure measured by the LP-TENG equals the last pressure plus the product of normalized movement direction and 5 kPa. Otherwise, the pressure does not change. Fig. S4a shows the first time the liquid column has crossed the negative electrode of NPN electrodes with the pressure increasing from 0.0 kPa to 5.0 kPa by FM. Fig. S4b displays the first time the liquid column has crossed the positive electrode of PNP electrodes with the pressure increasing from 5.0 kPa to 10.0 kPa by FM. Fig. S4c depicts the second time the liquid column has crossed the positive electrode of PNP electrodes with the pressure decreasing from 10.0 kPa to 5.0 kPa by BM. Fig. S4d presents the second time the liquid column has crossed the negative electrode of NPN electrodes with the pressure decreasing from 5.0 kPa to 0.0 kPa by BM. The experiment is demonstrated in Supplementary Video S3.

Supplementary material related to this article can be found online at doi:10.1016/j.nanoen.2023.108419.

Fig. 5e displays the schematic drawing and experimental results of the FV-TB-TENG of LP-TENG using four NPN electrode arrays for blood pressure (BP) sensing. The NPN electrode array can be regarded as a modified NP+PN electrode array, which combines two positive electrodes into a single positive electrode with a smaller size, higher resolution, and remaining amplified positive voltage. Here, the manometer is replaced by a mercury sphygmomanometer is used as the testing setup for BP monitoring. The NPN electrodes are respectively placed at the positions corresponding to the pressures of (120, 130, 140, and 160) mmHg. In Fig. 5e, the positive V_{oc} is 1–3 times larger than the negative V_{oc}. With the threshold voltage of 0.75 V, the V_{oc} can be modulated to square signals and peak signals like Fig. 5c. By accounting for the number of the peak signal, the BP can be obtained. With the known direction of the liquid column, the pressure is increasing when the liquid column moves forward by adding the number of the peak signal, and the pressure will be decreasing when the liquid column moves backward by subtracting the number of the peak signal. Concerning the systolic/diastolic blood pressure category, the NPN electrodes are respectively placed at the positions corresponding to the pressures of (80, 110, 120, 130, 140, and 160) mmHg. The experiment is demonstrated in Supplementary Video S4. The photograph of the LP-TENG using six NPN electrode arrays for BP detecting with a stepping motor or a cuff airbag is shown in Fig. 5f. Compared with the testing setup in Fig. 5a, the manometer has been replaced by a mercury sphygmomanometer. The BP test system here consists of a T-branch pipe, the LP-TENG, a mercury sphygmomanometer, the electrometer system, and a stepper motor or a cuff airbag. The stepper motor and the cuff airbag are used to simulate the BP pressure source by controlling the movement of the syringe plunger and the air pressure in the airbag, respectively. The T-branch pipe connects the syringe, the LP-TENG, and the mercury sphygmomanometer which is regarded as a reference detector of BP. The resolution ratio of LP-TENG for BP monitoring is higher than 10 mmHg, which can distinguish the BP level from the systolic blood pressure category.
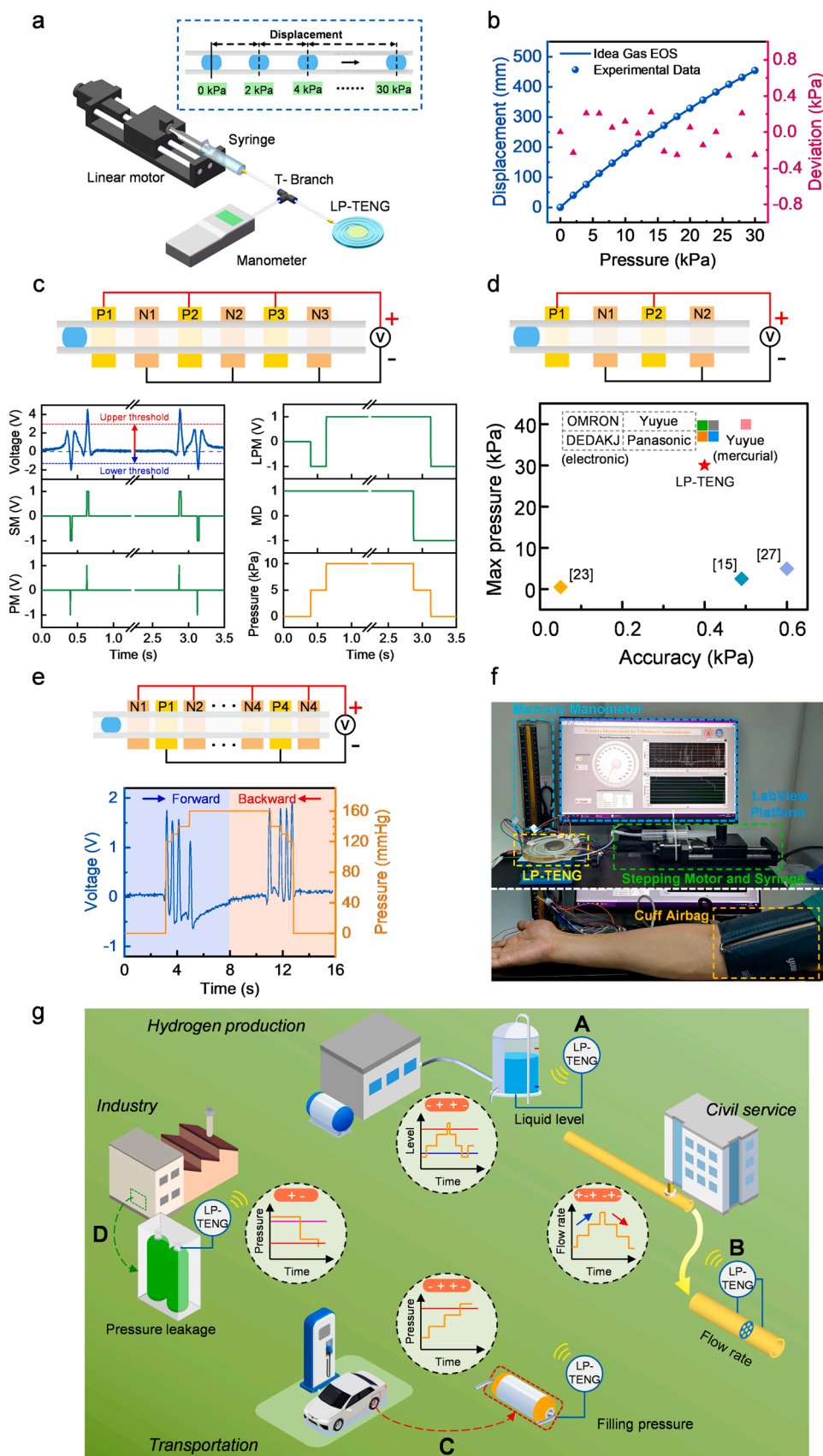
Fig. 5. Pressure sensing characteristics of LP-TENG using different electrode arrays. (a) Schematic representation of the testing setup for pressure sensing. (b) Relationship between the displacement of the liquid column and the determined pressure of LP-TENG. (c) The V_{OC}, square-modulated (SM) voltage, peak-modulated (PM) voltage, latest peak-modulated (LPM) voltage, Movement direction (MD), and the determined pressure of LP-TENG when the liquid column is crossing the PNP+NPN electrode array with the forward and then backward movement. (d) Comparison of the accuracy and the maximum pressure between LP-TENG using the PN+PN electrode array and several commercial products or literature results. (e) Schematic drawing and experimental results of LP-TENG using two NPN electrode arrays for blood pressure (BP) sensing. (f) Photograph of the LP-TENG using six NPN electrode arrays for BP detection with a stepping motor or a cuff airbag. (g) Schematic drawing of the LP-TENG with different electrode arrays for determining the pressure leakage, the liquid level, the flow rate, and the filling pressure.

Hence, the ability of BP monitoring for the level of systolic blood pressure category by LBP-TENG has been verified. The LP-TENG for BP monitoring is found to have the advantages of simple structure, easy expansibility, market competitiveness, low cost, and practical recovery. Besides, the schematic drawing of the LP-TENG with different electrode arrays for determining the pressure leakage, the liquid level, flow rate, and the filling pressure is shown in Fig. 5g. As a pressure sensor, the LP-TENG has a broad range of applications such as hydrogen production, civil service, industry, and transportation. For the liquid level alarming, when the liquid level reaches the warning line, the enhanced positive voltage detected by the LP-TENG with a NP+PN electrode array will also reach the alarm value. To detect the flow rate, based on the working principle of the orifice plate flow meter, the LP-TENG with PNP+NPN electrode arrays can be used to measure the pressure difference of the flowing fluid. For the filling pressure detection, the LP-TENG with NP+PN electrode arrays is able to measure the pressure of a fuel tank. If there is a pressure-leakage, the LP-TENG with a PN electrode array will show positive and then negative voltages, and the negative voltage will last for a long time to catch and hold people's attention.

Supplementary material related to this article can be found online at doi:10.1016/j.nanoen.2023.108419.

4. Conclusions

A LP-TENG with different electrode array structures has been demonstrated for self-powered fluid pressure sensing. The LP-TENG simply consists of a PTFE tube, a water droplet as a piston, copper electrodes, and a 3D printed air reservoir. When the LP-TENG is connected to a pressure source, the water droplet would move forward or backward to the air reservoir until the pressure of the pressure source and that of the air inside achieves equilibrium.

With a single channel detector, using the PN+PN electrode array, the accuracy of LP-TENG can reach around 0.4 kPa with a maximum pressure of 30 kPa. When the PNP+NPN electrode array is employed, the resolution ratio of the LP-TENG for BP pressure sensing is 10 mmHg, which is able to distinguish the BP level in the blood pressure category. Furthermore, with the developed computer software, it can easily determine the direction and the displacement of movement for the liquid column for real-time monitoring of the liquid flow status. Not only applied for liquid flow sensing, the flow sensor is also suitable for use with gases as well. Besides, the smart LP-TENG used as a pressure sensor has a broad range of potential applications, such as the one-off medical apparatus, hydrogen production, civil service, industry, and transportation.

5. Experimental section

5.1. Materials

The deionized water was purchased from Aladdin, and it was used without further purification. Transparent PTFE tubes (inner diameter = 2 mm, outer diameter = 2.4 mm) were bought from Oupli Company, China. Conductive copper tapes with a thickness of 60 μm were purchased from Yucheng Metal Material Company, China. The gas reservoir is made from titanium alloy by the 3D printer of Huashu FS271M with a deposition thickness of 0.03 mm.

5.2. Fabrication of device

Firstly, the PTFE tube was ultrasonically cleaned in ethanol for 8 mins, and then it was left in the drying oven at 40 ℃ for 30 mins. Secondly, the conductive copper tape was bonded to the outer wall of the PTFE tube as the external electrode. The volume of the gas reservoir is 4000 mm^3 with an inner diameter of 35.6 mm, an outer diameter of 37.6 mm, a height of 4.0 mm, and a thickness of 1.0 mm.

5.3. Characterization of the TENG

The electrical output performance of the tube-based TENG including the open-circuit voltage and the transferred charge were measured by an electrometer (Keithley 6514). A field-emission scanning electron microscopy (SU 3500) from the Instrument Analysis Center of Xi'an Jiaotong University was used to visualize the surface morphology of the PTFE tube's inner face. The software platform was constructed based on the LabView 2019, which is capable of realizing real-time data acquisition control and analysis.

CRediT authorship contribution statement

Taotao Zhan: Conceptualization, Methodology, Investigation, Data curation, Writing – original draft; **Haiyang Zou**: Conceptualization, Methodology, Supervision, Writing – review & editing; **Hengfei Zhang**: Investigation, Data curation, Visualization; **Peng He**: Methodology, Investigation; **Zhanlei Liu**: Investigation, Data curation; **Junshuai Chen**: Methodology, Investigation; **Maogang He**: Conceptualization, Investigation; **Ying Zhang**: Conceptualization, Supervision, Writing – review & editing; **Zhong Lin Wang**: Supervision, Writing – review & editing.

Declaration of Competing Interest

The authors declare that they have no known competing financial interests or personal relationships that could have appeared to influence the work reported in this paper.

Data availability

Data will be made available on request.

Acknowledgment

Appendix A. Supporting information

Supplementary data associated with this article can be found in the online version at doi:10.1016/j.nanoen.2023.108419.

References

[1] Z. Ullah, F. Al-Turjman, L. Mostarda, R. Gagliardi, Applications of artificial intelligence and machine learning in smart cities, Comput. Commun. 154 (2020) 313–323, https://doi.org/10.1016/j.comcom.2020.02.069.

[2] F. Al-Turjman, Information-centric framework for the Internet of Things (IoT): fraffic modeling & optimization, Future Gener. Comput. Syst. 80 (2018) 63–75, https://doi.org/10.1016/j.future.2017.08.018.

[3] J. Zhang, D.C. Tao, Empowering things with intelligence: a survey of the progress, challenges, and opportunities in artificial intelligence of things, IEEE Internet Things J. 8 (2021) 7789–7817, https://doi.org/10.1109/JIOT.2020.3039359.

[4] J.F. Sun, L.J. Zhang, Z.J. Li, Q. Tang, J. Chen, Y.Z. Huang, C.G. Hu, H.Y. Guo, Y. Peng, Z.L. Wang, A mobile and self-powered micro-flow pump based on triboelectricity driven electroosmosis, Adv. Mater. 33 (2021), 2102765, https://doi.org/10.1002/adma.202102765.

[5] F. Shen, Z.J. Li, H.Y. Guo, Z.B. Yang, H. Wu, M. Wang, J. Luo, S.R. Xie, Y. Peng, H.Y. Pu, Recent advances towards ocean energy harvesting and self-powered applications based on triboelectric nanogenerators, Adv. Electron. Mater. 7 (2021), 2100277, https://doi.org/10.1002/aelm.202100277.

[6] H.Y. Zou, L.T. Guo, H. Xue, Y. Zhang, X.F. Shen, X.T. Liu, P.H. Wang, X. He, G.Z. Dai, P. Jiang, H.W. Zheng, B.B. Zhang, C. Xu, Z.L. Wang, Quantifying and understanding the triboelectric series of inorganic non-metallic materials, Nat. Commun. 11 (2020) 2093, https://doi.org/10.1038/s41467-020-15926-1.

[7] X. He, H.Y. Zou, Z.S. Geng, X.F. Wang, W.B. Ding, F. Hu, Y. Zi, C. Xu, S.L. Zhang, H. Yu, M.Y. Xu, W. Zhang, C.H. Lu, Z.L. Wang, A hierarchically nanostructured cellulose fiber-based triboelectric nanogenerator for self-powered healthcare products, Adv. Funct. Mater. 28 (2018), 1805540, https://doi.org/10.1002/adfm.201805540.

[8] Z.Y. Wu, B. Zhang, H.Y. Zou, Z.M. Lin, G.L. Liu, Z.L. Wang, Multifunctional sensor based on translational-rotary triboelectric nanogenerator, Adv. Energy Mater. 9 (2019), 1901124, https://doi.org/10.1002/aenm.201901124.

[9] Z.M. Lin, B.B. Zhang, H.Y. Zou, Z.Y. Wu, H.Y. Guo, Y. Zhang, J. Yang, Z.L. Wang, Rationally designed rotation triboelectric nanogenerators with much extended lifetime and durability, Nano Energy 68 (2020), 104378, https://doi.org/10.1016/j.nanoen.2019.104378.

[10] F. Shen, D. Zhang, Q. Zhang, Z.J. Li, H.Y. Guo, Y. Gong, Y. Peng, Influence of temperature difference on performance of solid-liquid triboelectric nanogenerators, Nano Energy 99 (2022), 107431, https://doi.org/10.1016/j.nanoen.2022.107431.

[11] Q.T. Zhou, B.Y. Wang, A. long Gao, W.X. Xu, K. Zhou, J. Pan, G.W. Meng, C.F. Pan, F. Xia, Solution-tube-based volume effect triboelectric nanogenerator with salt and ph sensitivity, Adv. Funct. Mater. 32 (2022), 2209100, https://doi.org/10.1002/adfm.202209100.

[12] H.X. Zheng, H. Wu, Z.R. Yi, Y.X. Song, W.H. Xu, X.T. Yan, X.F. Zhou, S. Wang, Z.K. Wang, Remote-controlled droplet chains-based electricity generators, Adv. Energy Mater. 13 (2023), 2203825, https://doi.org/10.1002/aenm.202203825.

[13] T. Bhatta, P. Maharjan, K. Shrestha, S. Lee, Md Salauddin, M.T. Rahman, S.M.S. Rana, S. Sharma, C. Park, S.H. Yoon, J.Y. Park, A hybrid self-powered arbitrary wave motion sensing system for real-time wireless marine environment monitoring application, Adv. Energy Mater. 12 (2022), 2102460, https://doi.org/10.1002/aenm.202102460.

[14] Y. Qin, J.L. Mo, Y.H. Liu, S. Zhang, J.L. Wang, Q. Fu, S.F. Wang, S.X. Nie, Stretchable triboelectric self-powered sweat sensor fabricated from self-healing nanocellulose hydrogels, Adv. Funct. Mater. 32 (2022), 2201846, https://doi.org/10.1002/adfm.202201846.

[15] X.J. Cui, H.L. Zhang, S.L. Cao, Z. Yuan, J. Ding, S.B. Sang, Tube-based triboelectric nanogenerator for self-powered detecting blockage and monitoring air pressure, Nano Energy 52 (2018) 71–77, https://doi.org/10.1016/j.nanoen.2018.07.037.

[16] Z. Liu, Y. Ma, H. Ouyang, B.J. Shi, N. Li, D.J. Jiang, F. Xie, D. Qu, Y. Zou, Y. Huang, H. Li, C.C. Zhao, P.C. Tan, M. Yu, Y.B. Fan, H. Zhang, Z.L. Wang, Z. Li, Transcatheter self-powered ultrasensitive endocardial pressure sensor, Adv. Funct. Mater. 29 (2019), 1807560, https://doi.org/10.1002/adfm.201807560.

[17] J.Q. Xiong, H.S. Luo, D.C. Gao, X.R. Zhou, P. Cui, G. Thangavel, K. Parida, P.S. Lee, Self-restoring, waterproof, tunable microstructural shape memory triboelectric nanogenerator for self-powered water temperature sensor, Nano Energy 61 (2019) 584–593, https://doi.org/10.1016/j.nanoen.2019.04.089.

[18] D.Z. Zhang, Z.Y. Xu, Z.M. Yang, X.S. Song, High-performance flexible self-powered tin disulfide nanoflowers/reduced graphene oxide nanohybrid-based humidity sensor driven by triboelectric nanogenerator, Nano Energy 67 (2020), 104251, https://doi.org/10.1016/j.nanoen.2019.104251.

[19] Q.Q. Shen, X.K. Xie, M.F. Peng, N. Sun, H.Y. Shao, H. chuang Zheng, Z. Wen, X.H. Sun, Self-powered vehicle emission testing system based on coupling of triboelectric and chemoresistive effects, Adv. Funct. Mater. 28 (2018), 1703420, https://doi.org/10.1002/adfm.201703420.

[20] Z.Y. Zhu, K.Q. Xia, Z.W. Xu, H.J. Lou, H.Z. Zhang, Starch paper-based triboelectric nanogenerator for human perspiration sensing, Nanoscale Res. Lett. 13 (2018) 365, https://doi.org/10.1186/s11671-018-2786-9.

[21] X.Q. Zhang, M. Yu, Z.R. Ma, H. Ouyang, Y. Zou, S.L. Zhang, H.K. Niu, X.X. Pan, M.Y. Xu, Z. Li, Z.L. Wang, Self-powered distributed water level sensors based on liquid–solid triboelectric nanogenerators for ship draft detecting, Adv. Funct. Mater. 29 (2019), 1900327, https://doi.org/10.1002/adfm.201900327.

[22] B.D. Chen, W. Tang, C. He, T. Jiang, L. Xu, L.P. Zhu, G.Q. Gu, J. Chen, J.J. Shao, J.J. Luo, Z.L. Wang, Ultrafine capillary-tube triboelectric nanogenerator as active sensor for microliquid biological and chemical sensing, Adv. Mater. Technol. 3 (2018), 1700229, https://doi.org/10.1002/admt.201700229.

[23] M. Shahriar, C.P. Vo, K.K. Ahn, Self-powered flexible PDMS channel assisted discrete liquid column motion based triboelectric nanogenerator (DLC-TENG) as mechanical transducer, Int. J. Precis. Eng. Manuf. -Green. Technol. 6 (2019) 907–917, https://doi.org/10.1007/s40684-019-00148-8.

[24] Y. Wang, Z. Wang, D. Zhao, X. Yu, T. Cheng, G. Bao, Z.L. Wang, Flow and level sensing by waveform coupled liquid-solid contact-electrification, Mater. Today Phys. 18 (2021), 100372, https://doi.org/10.1016/j.mtphys.2021.100372.

[25] S.B. Jeon, M.L. Seol, D. Kim, S.J. Park, Y.K. Choi, Self-powered ion concentration sensor with triboelectricity from liquid-solid contact electrification, Adv. Electron. Mater. 2 (2016), 1600006, https://doi.org/10.1002/aelm.201600006.

[26] S.Y. He, Z. Wang, X.S. Zhang, Z.T. Yuan, Y.S. Sun, T.H. Cheng, Z.L. Wang, Self-powered sensing for non-full pipe fluidic flow based on triboelectric nanogenerators, ACS Appl. Mater. Interfaces 14 (2022) 2825–2832, https://doi.org/10.1021/acsami.1c20509.

[27] X.L. Zhang, Y.B. Zheng, D.A. Wang, F. Zhou, Solid-liquid triboelectrification in smart U-tube for multifunctional sensors, Nano Energy 40 (2017) 95–106, https://doi.org/10.1016/j.nanoen.2017.08.010.

[28] L. Pan, J.Y. Wang, P.H. Wang, R.J. Gao, Y.C. Wang, X.W. Zhang, J.J. Zou, Z.L. Wang, Liquid-FEP-based U-tube triboelectric nanogenerator for harvesting water-wave energy, Nano Res. 11 (2018) 4062–4073, https://doi.org/10.1007/s12274-018-1989-9.